Vesicle Formation and General Phase Behavior in the Catanionic Mixture SDS−DDAB−Water. The Cationic-Rich Side

Eduardo F. Marques,[†,§] Oren Regev,[‡] Ali Khan,[*,†] Maria da Graça Miguel,[§] and Björn Lindman[†]

Physical Chemistry 1, Center for Chemistry and Chemical Engineering, P.O. Box 124, Lund University, Lund S-221 00, Sweden, Department of Chemical Engineering, Ben-Gurion University, P.O.Box 653, 84105 Beer-Sheva, Israel, and Departamento de Química, Universidade de Coimbra, 3049 Coimbra, Portugal

Received: March 10, 1999; In Final Form: June 14, 1999

The phase behavior in the cationic-rich side of the phase diagram of the mixed system sodium dodecyl sulfate (SDS)−didodecyldimethylammonium bromide (DDAB)−water at 25 °C is presented. DDAB is a double-chained surfactant and thus it tends to self-assemble in water into bilayer structures−vesicles and lamellar phases. The phase diagram of the binary system DDAB−water has been studied, and some features of the diluted region as revealed by surfactant NMR self-diffusion and light microscopy are shown. The structural and phase behavior effects resulting from the addition of SDS are then investigated by complementary microscopy and NMR methods. Upon adding SDS to DDAB dispersions, the area for which a single phase of vesicles occurs is largely extended and a lobe is defined in the phase diagram. The DDAB-rich vesicles are essentially unilamellar and characterized by large sizes (range 0.1−5 μm) and high polydispersity, as probed by combined cryo-TEM and light microscopy. Self-diffusion measurements show a nonmonotonic variation of water self-diffusion coefficients with the molar fraction of SDS in the mixture, which is correlated to a nonmonotonic variation of mean vesicle size. Microscopy results support this picture. The trends are qualitatively reproduced if initially sonicated (nonequilibrium) DDAB vesicles are used to prepare the catanionic mixtures. The observations are rationalized in terms of an interplay between two opposing effects associated with the presence of SDS in the bilayer−electrostatic effects and packing effects.

I. Introduction

The formation of stable vesicle phases in aqueous mixtures of cationic and anionic surfactants (catanionic mixtures), without recourse to highly energetic methods such as sonication and extrusion, is perhaps the most outstanding feature of the phase behavior of these systems, in the dilute regime. In the past decade several authors have presented experimental evidence for vesicle formation in catanionic systems[1−7] and theoretical modeling has also been put forth,[8−10] in close connection with the experimental observations. In a previous work,[7] a global view of the phase behavior of the catanionic system sodium dodecyl sulfate (SDS)−didodecyldimethylammonium bromide (DDAB)−water was presented at 25 °C in the very dilute region. Emphasis was placed in the detailed characterization of phase microstructure in the SDS-rich side of the system. In the current work, the complementary investigation of the cationic surfactant-rich side is presented.

The system of interest here can be seen as a case study for catanionic mixtures, since both electrostatic and geometric packing effects are at play in the dictation of self-assembly. Because of its strong hydrophobicity, the DDAB molecule has very low solubility in water and its packing parameter dictates a preference to assemble into bilayer-based structures.[11,12] Thus, the surfactant readily displays lamellar liquid crystal formation in water[13−16] and, at low concentrations, complex equilibria involving giant onion structures and uni- and bilamellar vesicles.[17−21] The formation of vesicular structures also in the DDAB-rich area of the catanionic system is thus expected, since they occur already in the binary system DDAB−water. Less predictable is the effect of adding the anionic single-chain amphiphile on the particular sequence of structures forming (shape, size, polydispersity) and, consequently, in the complete phase behavior picture. While electrostatic interactions are the main driving force for the association between the two surfactants, they are modulated by the packing requirements derived from the different molecular geometry of the two amphiphiles. The concentration of salt (NaBr) in the system, which varies as the mixing ratio between the surfactants is varied, may also influence phase stability and structure.

The very low concentration of monomeric surfactant in the present type of mixtures implies that equilibration rates, which undergo via monomer exchange, may be rather slow. Days, weeks, or months may be necessary before a bilayer-based system reaches equilibrium, in contrast to the labile micellar system. In such cases, time and the historical treatment of the sample may be of importance in terms of phase behavior determination and also of the structural details of the phases, as will be shown further. Finally, we note that there is an analogy between the current work and studies on the solubilization or disintegration process of vesicles prepared from phospholipids (which are commonly double-chained amphiphiles) by the addition of single-chain surfactants.[22−24] These studies are directly relevant to protocols for membrane reconstitution of proteins in biological research and pharmacological applications.

* Email: ali.khan@fkem1.lu.se Fax: +46 46 222 4413 tel: +46 46 222 3247

[†] Lund University.

[‡] Ben-Gurion University.

[§] Universidade de Coimbra.

10.1021/jp990852p CCC: $18.00
Published on Web 09/15/1999

A basic distinction between our approach and the majority of the latter reports is that we aim at a detailed phase behavior study.

II. Experimental Section

A. Materials and Sample Preparation. SDS and DDAB of high purity were obtained from BDH and Tokyo Kasei, respectively, and used without further purification. Millipore water was used in all samples. The composition of samples is given by surfactant weight percentage, or when more convenient for some measurements in terms of total molar concentration, $C_t = C_{SDS} + C_{DDAB}$, and by the molar fraction of SDS in the mixture, $X_{SDS} = C_{SDS}/(C_{SDS} + C_{DDAB})$. Depending on sample composition and the nature of measurements to be carried out, three different methods of sample preparation were used. (i) Samples with more than 1 wt % DDAB were prepared by weighing directly the two surfactant solids into glass tubes and thoroughly mixing them in water. (ii) Samples with less than 1 wt % DDAB were mixed by weight from a SDS micellar solution and a DDAB *dispersion* which was carefully homogenized. When the total surfactant molar concentration, C_t, was to be kept constant in a series of samples they were mixed by volume. (iii) Series of samples at constant C_t and increasing X_{SDS} were also mixed by volume from a SDS micellar solution and a DDAB *solution*. This solution was obtained by sonication of a homogenized lamellar dispersion. Sonication of 10 mL aliquots of a DDAB turbid dispersion with an ultrasonicating tip probe for a period of 10 min, at 25 °C, produces a bluish and transparent solution. A Vibra Cell 300 ultrasonic processor from Sonic & Materials (USA) was used, with a probe containing an ultrahigh-intensity stepped Ti microtip (3 mm in diameter).

B. Phase Diagram Determination. After preparation, the samples were left for equilibration prior to the examination of phase behavior. Inspection between crossed polaroids followed in order to search for birefringent phases. Equilibration times are particularly long for surfactants having low monomer solubility, such as DDAB. Lamellar dispersions of DDAB may take days to weeks before they separate into two coexisting phases. All samples were left undisturbed and observed in the course of at least three months in order to check for phase separation phenomena, such as flocculation or precipitation.

C. Surface Tension. The surface tension measurements for DDAB solutions were made by the du Noüy platinum ring method at 25 °C.

D. Light Microscopy. Under polarized light, optically isotropic phases show as a dark background in the microscope, while anisotropic phases show distinctive textures. Lamellar dispersions containing large multilamellar vesicles (onions) show domains with a characteristic Maltese cross pattern under polarizing light.[25] Many surfactant aggregates are inherently of low contrast and so they cannot be easily distinguished from the background if normal light is used in a light microscope; moreover, the use of visible light puts a lower limit to resolution. If a microscope is equipped with (i) differential interference contrast (DIC) lenses and (ii) a TV camera connected to the microscope, both contrast and resolution can be improved in what is termed differential interference contrast video-enhanced microscopy (DIC−VEM).[18,26] This technique is optimal to detect μm-sized vesicle structures with normal light.[12] An Axioplan Universal polarizing light microscope from Carl Zeiss, equipped with DIC lenses and a video camera system (Dage−MTI, model VE-100), was used.

E. Cryo-Transmission Electron Microscopy. Cryo-TEM is a particularly suitable technique for the direct visualization of surfactant aggregates ranging in size from about 5−10 nm to 1 μm. The samples were prepared and transferred according to the usual procedure. The sample is placed in the controlled environment vitrification chamber at room temperature,[27] where relative humidity is kept close to saturation to prevent water evaporation from the sample. A 5 μL drop of the solution is put on a carbon-coated holey film[28] supported by a TEM copper grid. After gently blotting the drop with filter paper in order to create a thin liquid film over the grid, this one is rapidly plunged into liquid ethane at its melting temperature, so that a vitrified film is obtained. The vitrified specimen is then transferred under liquid nitrogen environment by use of a cold stage unit (model 626, Gatan Inc., Warrendale, PA) into the electron microscope. A JEOL 2000FX operating at 100 kV with a nominal underfocus of 4 μm was used. The working temperature was kept below −168 °C and the images were recorded on Kodak SO-163 film.

F. NMR Pulsed Field Gradient (PFG) Self-Diffusion. The PFG technique for measuring self-diffusion coefficients is based on a combination of a sequence of radio frequency (rf) pulses leading to the formation of spin−echoes and magnetic field gradient pulses which "label" the spins magnetically.[29,30] In the method, one monitors the attenuation of a spin−echo resulting from the dephasing of the nuclear spins due to the combined effect of translational motion of the spins and the imposition of the gradient pulses. The self-diffusion coefficient of the diffusing spins can thus be directly extracted from the echo attenuation. The typical PFG sequence is based on the Hahn spin−echo and is known as the Stejskal−Tanner experiment. The Hahn echo sequence consists of two rf pulses: a 90° pulse applied at time $t = 0$ and a 180° pulse at time $t = \tau$ gives rise to an echo signal at $t = 2\tau$ because of a refocusing of the transverse magnetization. In addition to these rf pulses, two field-gradient pulses are applied with time duration δ and separation Δ between their leading edges, placed on either side of the 180° rf pulse. The echo intensity at time 2τ for Gaussian diffusion is given by the Stejskal−Tanner equation

$$I(2\tau) = I_o\, e^{-2\tau/T_2}\, e^{-\gamma^2 g^2 \delta^2 (\Delta - \delta/3) D} \qquad (1)$$

where I_o is the echo intensity for $\delta = 0$, T_2 is the transverse relaxation time, γ is the proton magnetogyric ratio, g is the magnitude of the gradient pulse, D is the self-diffusion coefficient and τ, δ, and Δ are as defined above. Since the time τ is kept constant, the relaxation term $2\tau/T_2$ is also constant and can be included in I_o, so that eq 1 can be simplified to

$$I(k) = I'_o\, e^{-kD} \qquad (2)$$

where $k = (\gamma \delta g)^2(\Delta - \delta/3)$. The diffusion coefficient can be readily determined by measuring the intensity decay of a Fourier transform starting at the center of the echo (echo attenuation) as a function of g, δ, or Δ. Usually, the echo attenuation is measured as a function of δ, at constant gradient strength g and pulse separation Δ. In the stimulated echo sequence, which is used alternately to the Hahn echo in spin systems with short T_2 values, three 90° rf pulses are used and the field gradient pulses are switched on before the second and after the third rf pulse.[29,30]

The measurements were done in a Bruker DMX200 spectrometer, operating at a ^{1}H resonance frequency of 200 MHz, with a gradient probe providing a maximum field gradient of 8.8 T/m. For the monitoring of the water self-diffusion the basic Hahn echo pulse sequence was used. The surfactant self-diffusion was measured in very dilute binary DDAB−water solutions by means of the stimulated echo pulse sequence. D_2O

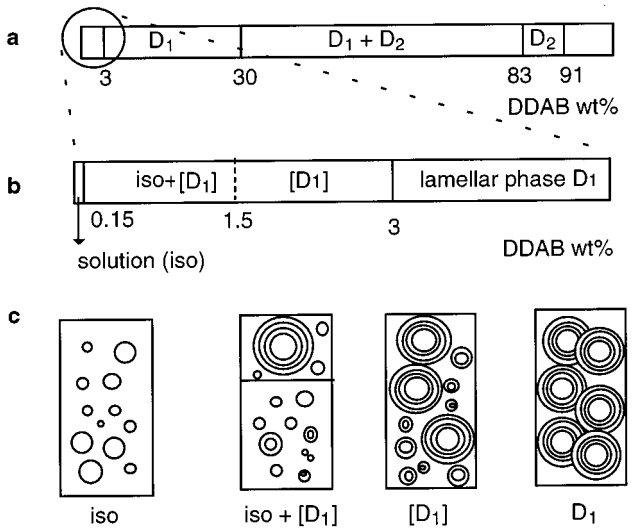

Figure 1. Phase behavior of the DDAB−water system at 25 °C. (a) Over the entire composition range, where D_1 is the dilute (or swollen) lamellar phase and D_2 is the concentrated (or collapsed) lamellar phase. (b) The dilute region shown in detail. Iso stands for isotropic solution. [D_4] is a stable dispersion of D_1 domains in the iso phase (see also text). (c) Schematic view of the sequence of structures.

supplied by Dr. Basel, Switzerland, was used in the latter samples. The number of scans run for each magnitude of the gradient strength g_z varied between 256 for the most concentrated sample, 0.14 wt % DDAB, and 1024 for the most dilute one, 0.005 wt % DDAB.

III. Results and Discussion

The determination of the phase behavior and aggregate structure for the pseudoternary system DDAB−SDS−water requires an initial overview of the same aspects for the binary DDAB−water system. DDAB is a typical swelling surfactant,[31] in contrast to soluble micellar-forming amphiphiles, and, as will be shown below, its aqueous phase behavior presents some unusual features, both in the concentrated and in the dilute regions.

A. The Dilute Binary System DDAB−Water. *1. Phase Behavior.* Over the full concentration range and above its chain melting temperature, neat DDAB displays in water a rich and complex phase behavior, as experimentally observed by several groups.[13,14,16] At 25 °C, the surfactant forms two lamellar phases in water (Figure 1a): (i) a concentrated (or collapsed) lamellar phase, D_2, between 83 and 91 wt % surfactant, with a *d*-spacing of about 3.2 nm; (ii) a dilute (or swollen) lamellar phase, D_l, between 3 and 30 wt %. The two lamellar phases are in equilibrium in a wide two-phase region, which shrinks as the temperature is raised until a critical point is attained.[16] In the very dilute region, the surfactant forms a bluish isotropic solution until about 0.15 wt % (≈3.2 mM) at 25 °C. The dilute lamellar phase, D_1, shows as a strongly birefringent liquid crystal under polarized light. In the range 0.15−3 wt % a two-phase region is present, containing the isotropic solution and the lamellar phase D_1. The macroscopic appearance of the biphasic region is dependent on the surfactant concentration and time left for equilibration, as will be discussed below. For lower concentrations and short equilibration times the two-phase region shows macroscopically as a pseudoisotropic region commonly designated as a *lamellar dispersion*. The complete phase behavior of DDAB in water at 25 °C is schematically depicted in Figure 1. The formation of a variety of vesicular structures in DDAB dispersions was recognized by Ninham and co-workers[18,26] long ago, and thereafter a number of detailed structural and phase behavior work has been reported.[15,19−21] The surfactant microstructure in the different phase regions is reviewed below on the basis of the above reports and complementary observations made in this work.

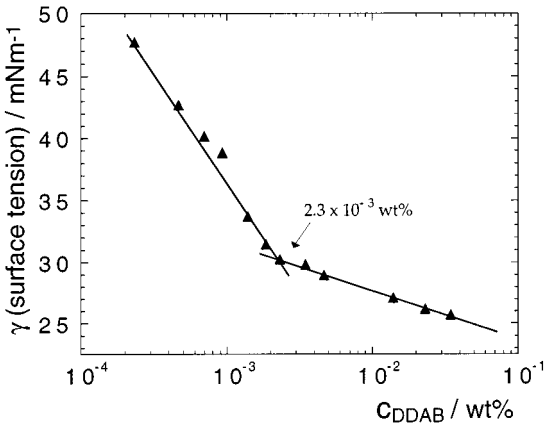

Figure 2. Surface tension vs surfactant concentration for DDAB solutions at 25 °C.

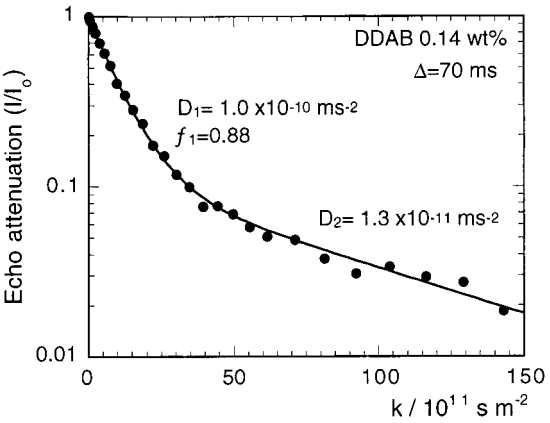

Figure 3. Echo-decay plot for a DDAB solution at 0.14 wt % for a Δ value of 70 ms. The two self-diffusion coefficients for surfactant obtained from a biexponential fit are shown (see also Table 1).

2. Phase Microstructure. a. Solution Phase (c < 0.15 wt % DDAB). In Figure 2 a plot of the surface tension (γ) of DDAB solutions vs surfactant concentration (log *c*) is shown. A clear break is observed at ca. 2.3×10^{-3} wt % (≈0.050 mM), in good aggreement with values previously reported.[21,32,33] The observed break defines a critical aggregation concentration (CAC) for DDAB. Given the fact that the packing parameter of the surfactant, as usually defined,[11,34] is close to 1,[14,35] the formation of spherical micelles at the break in the γ-log *c* plot, typical for the usual single-chained amphiphiles, is rather unfavorable. To investigate the nature of DDAB self-assembly at such low concentrations, surfactant NMR self-diffusion measurements were carried out in this work.

The surfactant diffusion was monitored for a few concentrations between the break and the solution boundary, at 0.15 wt % DDAB. The main methylene peak of the surfactant was followed in solutions prepared in D_2O. The echo-decay in Figure 3, for 0.14 wt % DDAB, is representative of the self-diffusion data obtained. The echo-decay is clearly nonexponential, showing a fast- and a slow-diffusing component. The data were fitted with a biexponential decay and the two values, D_{fast} and D_{slow}, obtained. Table 1 lists the *D* values obtained from biexponential fits to the echo-decay for lower concentrations. We note that the fit error for D_{slow} is somewhat large because

TABLE 1: Surfactant Self-diffusion Coefficients for DDAB Solutions at 25 °C from Biexponential Fits to Experimental Data Obtained with PFG−NMR

DDAB wt %	$D_{fast}/10^{-10}$ m^{2}s^{-1}	$D_{slow}/10^{-11}$ m^{2}s^{-1}	R_H calcd from D_{slow}/nm
0.14	1.04 ± 0.02	1.3 ± 0.1	16
0.05	1.14 ± 0.02	1.5 ± 0.2	12
0.02	1.41 ± 0.02	2.4 ± 0.4	8.3
0.005	2.67 ± 0.06		

of the low signal-to-noise ratio for the slow-diffusing component. For the most dilute solution investigated, 0.005 wt %, only one D value was obtained and D_{slow} could not be detected. The results in Figure 3 and Table 1 point to the existence of (a) two distinct *diffusing sites*, with diffusion coefficients D_{fast} and D_{slow}; (b) slow exchange of monomer between the sites in the experimental time scale, 70 ms in this case.

In the PFG experiment, the measured diffusion coefficient is a time-averaged value between the diffusion coefficients of aggregated (bound) and monomeric (free) surfactant

$$D_{meas} = p_{bound}D_{aggregate} + (1 - p_{bound})D_{free} \quad (3)$$

At 0.14 wt %, the fraction of monomeric surfactant is negligible, since $c \gg$ CAC; thus, the contribution of monomeric surfactant diffusion to the measured D_{slow} and D_{fast} for that concentration can be neglected. The particle hydrodynamic radius, R_H, can be obtained from $D \approx D_{aggregate}$ by the Stokes−Einstein equation

$$R_H = \frac{k_B T}{6\pi\eta D} \quad (4)$$

where k_B is the Boltzmann constant, T is the absolute temperature, η is the solvent viscosity, and R_H is the hydrodynamic radius. If then one inspects the D_{fast} values in Table 1, a significant observation is that at 0.14 wt % DDAB, D_{fast} is consistent with the diffusion of an aggregate much smaller than a vesicle. In fact, using $\eta = 1.12 \times 10^{-3}$ Kg m^{-1} s^{-1} for D_2O, an R_H value of 1.9 nm is obtained, which is consistent with the size of a *micelle*. For 0.05 and 0.02 wt % DDAB, D_{fast} is already weighted by the contribution of monomeric surfactant, since the value obtained is 10−40% larger than typical D values for micellar aggregates. With respect to D_{slow}, the values are compatible with the translational diffusion coefficient of aggregates much larger than a typical micelle and indeed consistent with that of small vesicles (Table 1). Furthermore, if at 0.02 wt % and 0.05 wt % DDAB the weight of $p_{free}D_{free}$ in D_{slow} is neglected (i.e., if slow monomer−vesicle exchange is assumed), then an increase in the vesicle radius from 8.3 to 16 nm is observed from 0.02 to 0.14 wt % DDAB (Table 1).

Therefore, with the data available from the above measurements there is evidence for the formation of micelles at the break in the γ-log c plot, in which case the latter can denote a true CMC for the surfactant. Also, the data indicates the coexistence of micelles and vesicles in the solution region for CMC$< c <$0.15 wt %. It is likely that the region of micelle-only formation is very narrow in terms of concentration range. A significant observation in Figure 2 is that over 1 order of magnitude above the break there is a small decrease in the surface tension, indicating that the monomer activity does not remain exactly constant until the solution boundary is attained.

It should be pointed out that small unilamellar vesicles with diameters in the range of 30−40 nm were detected for very dilute DDAB samples in the solution region, by direct imaging methods such as cryo-TEM[20] and freeze−fracture TEM.[21] The vesicles are structurally identical to the sometimes cited asymmetric L_3 (sponge) phase.[21,32] These observations favored the view of vesicle formation at the break in the γ-log c plot and thus the notion of a critical vesicle concentration, CVC, for DDAB has been used by several authors.[21,33] However, it is very likely that the direct imaging methods used are not able to detect the small number of micellar aggregates in such dilute solutions of DDAB ($c <$ 0.15 wt %), which can be detected by the more sensitive self-diffusion NMR technique. Light scattering measurements have also been done in dilute DDAB solutions, in the range 0.01−0.1 wt % DDAB,[36] and they revealed (i) the presence of a slow- and fast-diffusing component; (ii) a hydrodynamic radius of ≈35 nm for the slow component (consistent with a vesicle size); (iii) a significant increase in scattering at about 0.025 wt %. The appearance of a fast-diffusing component and the measured increase in scattering (attributed to an increase in vesicle size) are in qualitative agreement with our results from NMR surfactant self-diffusion (Table 1).

Overall, the data obtained by us and from previous reports can be summed up in the following way: (i) at the break in the γ-log c plot, the CAC for the surfactant, DDAB assembles into small aggregates of micellar size and a region of micelle−vesicle coexistence is detected by self-diffusion NMR for CAC$< c <$0.15 wt %; (ii) small unilamellar vesicles of about 20−40 nm in radius are observed by several techniques for CAC$< c <$0.15 wt %; (iii) with an increase in concentration within the solution region, there is an increase in vesicle size.

The detection of regions of micelle−vesicle equilibrium has been extensively reported before for didodecyldimethylammonium surfactants having less usual counterions, such as hydroxide (DDAOH) and acetate (DDAAc).[17,18,37] In fact, these double-chained surfactants have the peculiarity of being highly soluble in water, prior to lamellar phase formation. Upon increasing concentration within the isotropic phase they show a sequence of structures of vesicles→coexisting vesicles and micelles→micelles. This counterintuitive sequence, which has been termed "super-aggregation" and accounted for previously on the basis of strong counterion hydration for these surfactants,[18,38] appears then to be the inverse of that observed here for DDAB. We also note that Miller et al. have suggested a vesicle-to-micelle transition at high temperatures for dilute dispersions of double-chained surfactants with bromide and chloride counterions.[18] It seems then clear, in the context of these reports and our observations, that further detailed investigation of the aggregation behavior of the highly diluted region of the DDAB−water system is needed.

*b. Two-Phase Region (0.15 < c <*3 wt %). By adding DDAB in water in the range of 0.15−1.5 wt % surfactant, a bluish turbid dispersion is initially formed. The dispersion shows birefringence under flow and remains macroscopically homogeneous for 1 to 4 weeks, depending on concentration. After this period of time, a visible phase separation takes place: a flow birefringent layer is formed at the top of a turbid solution. The time for equilibration and the volume fraction of the upper phase increase with concentration. The microstructure in this region has been revealed by electron microscopy techniques.[19,20] The observations indicate that the lower phase, the bluish solution, contains essentially large unilamellar vesicles (LUVs) with a mean diameter of 200 nm, between 0.15 and 0.5 wt % DDAB. Between 0.5 and 1.5 wt %, the unilamellar vesicles are replaced with large bilamellar vesicles, i.e., vesicles with two concentric bilayers, in the range 100−600 nm, having a characteristic distance of 25 nm between the two layers.[20] As for the nature of the upper phase, light microscopy observations

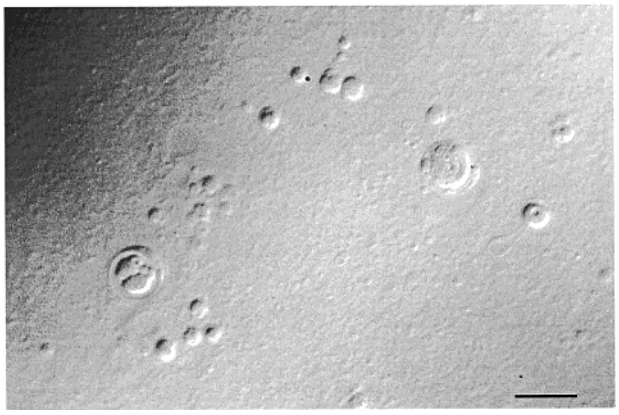

Figure 4. Imaging by light microscopy of the upper birefringent phase of a 0.7 wt % dispersion of DDAB in water (≈ 15 mM); bar = 10 μm.

in this work show the presence of large vesicular (10 μm sized) structures, as can be seen in Figure 4 (for a 0.7 wt % DDAB dispersion), in a "sea" of smaller vesicles (less than 1 μm).

Between 1.5 and 3 wt % DDAB the dispersions appear as homogeneous and intensely bluish to the naked eye, but between crossed polaroids they yield static birefringence and a lustrous, rainbowlike display of colors (iridiscence). No macroscopic phase separation takes place with time, not even after ultracentrifugation. Dubois and Zemb have shown that for such compositions the system is still biphasic, despite its homogeneous appearance; it contains the lamellar phase D_1 in equilibrium with the isotropic solution.[15] The region is indicated by [D_1] in Figure 1 and in fact it consists of a very stable dispersion of lamellar (D_1) "domains"—large multilamellar vesicles (MLVs or onions)—in the "excess water" phase, a dilute solution containing tubular structures and bilamellar vesicles (100−200 nm). Probably because of a balance in density the two phases do not separate macroscopically.

c. Lamellar Phase D_1. Between approximately 3 wt % and 30 wt % DDAB, a lamellar phase forms, built up of micron-sized multilamellar vesicles which occupy all the available volume. All of the compositions within this range show strong static birefringence without iridiscence. They are rather viscous, since the flow requires sliding and deformation of the onion structures. In the polarizing light microscope, typical Maltese cross patterns appear in a dark background.[39] The D_1 phase is characterized by a linear swelling between 30 and 3 wt %, with a repeat distance d increasing from 10 to 80 nm,[15] while the bilayer thickness remains constant at 2.4 nm. By performing careful osmotic pressure measurements and numerically estimating the forces between bilayers, Zemb et al. have shown a mechanism for the minimum and maximum swelling observed for this dilute DDAB−water lamellar phase.[32] In particular, it has been shown that the maximum swelling occurs when the osmotic pressure of the lamellar phase equals that of the isotropic vesicular phase, and this coexistence plateau value is independent of the concentration of added salt.[32]

Two characteristic lengths are associated with the lamellar phase: (i) the repeat distance d and (ii) an average distance between the centers of two neighboring onions. The observed iridescence occurs when the wavelength of visible light matches the Bragg condition associated with the distance between the onion superstructures. The lamellar dispersion [D_1], mentioned above, was inferred from SAXS measurements,[15] since a repeat distance d less than the predicted value for linear swelling was obtained for the pseudohomogeneous samples of that region.

A schematic phase diagram for DDAB in water at 25 °C in the dilute region is presented in Figure 1b and c, summarizing the preceding observations.

B. Phase Behavior in the DDAB-Rich Side of the Dilute Catanionic System. SDS is a surfactant with a packing parameter of ca. 1/3 and so the optimal aggregate for the molecule is a roughly sphericall micelle. The addition of SDS to the bilayer-biased DDAB−water system is thus expected to have relatively strong effects on the phase behavior and microstructure of the surfactant system. In the phase diagram over the full concentration range, the effects are dependent on the total surfactant concentration. The concentrated lamellar phase, D_2, can be stabilized by the addition of SDS and eventually a cubic phase is formed in the vicinity of equimolar ratios between the two surfactants.[40] The dilute lamellar phase, D_1, is destabilized by trace amounts of SDS and the effect is similar to a salt effect. In fact, addition of NaBr has been shown to "shrink" the existence region of the D_1 phase, mainly because of electrostatic screening effects.[15,41] On one hand, the addition of SDS induces both a surface charge neutralization (screening of the headgroup repulsions) and, more importantly, a release of the counterions from the aggregate surface into the bulk, with a consequent screening of the double layer repulsions. On the other hand, the introduction of a single-chained surfactant in the bilayer creates packing constraints which tend to favor highly curved aggregates. The electrostatic and the packing effects oppose each other. Overall, it seems reasonable to expect a nonmonotonic variation of aggregate curvature as the molar ratio of SDS increases in the mixture toward equimolarity.

1. Isotropic Solution Region. On addition of SDS, the bluish isotropic solution expands to much higher surfactant concentration as compared to the binary DDAB−water system. This can be seen in Figure 5a and b, where the phase diagram of the dilute mixture in the DDAB-rich side is shown in detail. The solution region takes up to a maximum of ca. 0.76 wt % DDAB and forms only within a limited range of X_{SDS}, the molar fraction of SDS in the surfactant mixture. Between 0 and 0.25 wt % DDAB, a solution is present even for trace amounts of added SDS. As the DDAB concentration increases from 0.25 to 0.76 wt %, the solution region forms for an increasing value of X_{SDS}; below this value the biphasic region occurs. A single-phase lobe is thus defined in the phase diagram in Figure 5. The solution is rather turbid and when turned between crossed polaroids yields a weak birefringence. The upper limit of X_{SDS} for solution formation, i.e., the solution boundary line, occurs at a constant value of $X_{SDS} = 0.23$ (Figure 5b). For $X_{SDS} > 0.23$, phase separation occurs, with the appearance of catanionic crystals at the top of the solution. The phase boundaries are shown on the basis of ocular inspections of samples which remain unchanged for months.

2. Heterogeneous Regions. Upon SDS addition to the dilute DDAB−water system, three heterogeneous regions can be identified, as apparent in Figure 5: two biphasic regions and a three-phase region. At low X_{SDS} values, the lamellar dispersion is still present and it shows as a turbid solution at the top of which a flow birefringent phase forms (first biphasic region—*sol* + *lam*). At higher X_{SDS}, closer to equimolarity, crystals are in equilibrium with a turbid solution where no birefringent domains can be detected, implying that the lamellar phase is absent (second biphasic region—*sol* + *cryst*). Between 0.25 wt % and 0.76 wt % DDAB the biphasic regions are separated by the single solution phase. Above 0.76 wt % DDAB they are separated by a narrow three-phase region, composed of the lamellar dispersion and crystals. Evidence for the latter region comes from more surfactant-concentrated samples (more than 2 wt % DDAB) which display three distinct phases: a lower

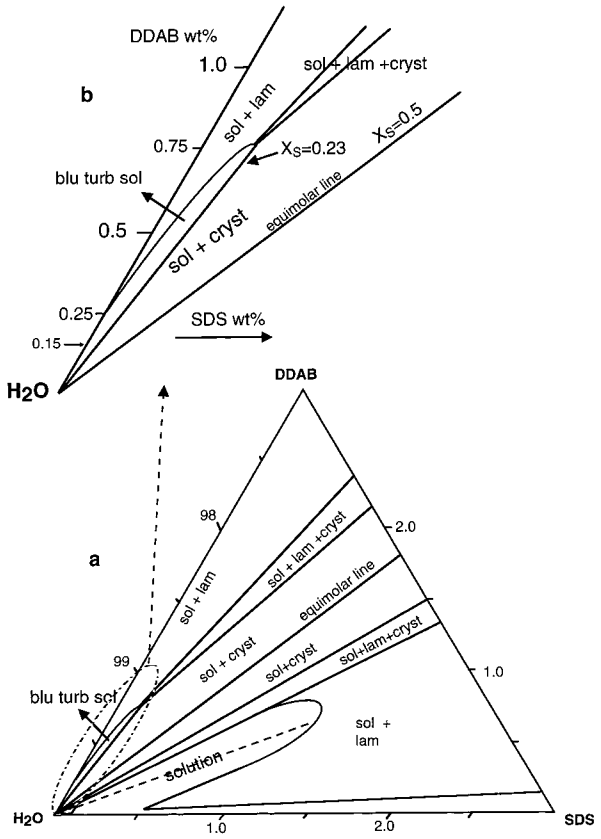

Figure 5. Phase behavior for the catanionic mixture SDS−DDAB−water at 25 °C in the dilute region (total surfactant concentration less than 3 wt %): (a) general view; (b) detailed view of the phase behavior in the DDAB-rich side. Abbreviations: blu, bluish; turb, turbid; sol, solution; lam, lamellar phase; cryst, crystals.

turbid solution, a middle phase showing strong static birefringence (lamellar phase), and an upper phase containing dispersed crystallites (catanionic solid). The lamellar dispersions with 2−3 wt % DDAB and no added SDS are strongly static birefringent, appear macroscopically homogeneous, and are rather viscous. As SDS is gradually added, the samples show an increasingly weak flow birefringence and the viscosity decreases markedly.

C. Phase Structure by Microscopy and Self-Diffusion Methods. *1. Overview.* Structural characterization of the DDAB-rich dispersions and solutions was carried out both by cryo-TEM and video-enhanced light microscopy. The combination of both techniques allows a full assessment of size polydispersity in the samples. The detailed characterization was based on many cryomicrographs per sample and a few images have been selected to illustrate the main effects. Similar to the study done for the SDS-rich side,[7] both dilution paths and paths with variable surfactant mixing ratios at fixed total surfactant concentration were monitored. A global observation is that a rich diversity of vesicular aggregates occurs in the DDAB-rich side, in contrast to the anionic-rich side, in which mostly unilamellar vesicles were detected. Some other general features for the DDAB-rich vesicle solutions are apparent. (i) Both unilamellar vesicles and multilamellar vesicles are observed in most samples, and the size range is often broad. (ii) The unilamellar vesicles are in general large-to-giant in size, i.e., ranging from 100 to 1000 nm in diameter. (iii) Small unilamellar vesicles (SUVs) are present in fair amounts only for compositions below 0.4 wt % DDAB. (iv) Bilamellar vesicles (BLVs) are commonly observed structures, similar to the binary DDAB−water system.

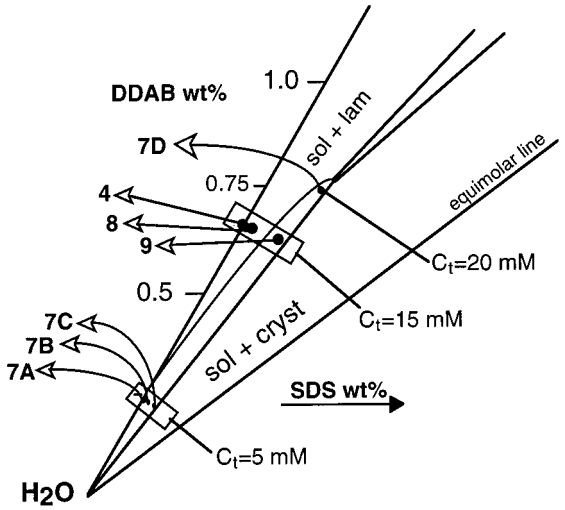

Figure 6. Location in the phase diagram of the SDS−DDAB−water system of the samples imaged in Figures 7, 8, and 9.

2. Microstructure Evolution Upon Addition of SDS. a. Microscopy. By increasing X_{SDS}, at constant total surfactant concentration, some effects are observed on the vesicle structures present in the dispersions and solutions. The effects will be illustrated by two series of samples at (i) $C_t = 5$ mM and (ii) $C_t = 15$ mM, the location of which can be seen in the phase diagram in Figure 6.

(i) The vesicles which are present in the dilute lamellar dispersion of neat DDAB, below 0.5 wt % surfactant, are characterized by a unilamellar structure and a mean diameter of 200 nm. At $C_t = 5$ mM and a very low amount of added SDS, $X_{SDS} = 0.02$, giant unilamellar vesicles (GUVs) 200−800 nm in diameter are found (Figure 7A). Some appreciable number of SUVs of 50−100 nm size can also be detected. Upon increasing X_{SDS} to 0.10, essentially SUVs 20−100 nm in diameter can be observed (Figure 7B). For this sample, only a sparse amount of very large vesicles, which characterized sample 7A, are found. Further increase of X_{SDS} to 0.17 shows that essentially SUVs and BLVs 100−250 nm in diameter are observed (Figure 7C). Another visible feature in the micrographs is the smoothness of the vesicle surface at lower X_{SDS}, seen in Figure 7A and B, as compared to the undulations of the bilayer seen at higher X_{SDS}, in Figures 7C and D (arrows).

(ii) For this series, the structural characterization was done both by cryo-TEM and light microscopy. At $X_{SDS} = 0$, the sample consists of a 15 mM neat DDAB dispersion which after a few days turns into a biphasic sample. The imaging of the top birefringent layer, composed of [D_1] domains, is shown in Figure 4. Clusters of flocculated large vesicles of 1−10 μm are clearly seen. These flocculae exist in a concentrated dispersion of large/giant vesicles, of maximum ca. 2 μm in size, as can also be seen in Figure 4. The bottom phase, the dilute isotropic solution, contains smaller vesicles with an average diameter of 200 nm.[20] At $X_{SDS} = 0.05$, the sample appears initially as a homogeneous dispersion but after a few days of equilibration a flow birefringent layer forms at the top, similar to the previous composition. The cryo-TEM micrographs shown in Figures 8A and B were obtained for the dispersion. Essentially very large vesicle structures (0.2−1 μm) are observed, with dominance of polydisperse BLVs (Figure 8A and 8B). To be noticed is the gradient in the mass thickness contrast of the film, observed on going from the center (where the electron beam crosses four bilayers) to the outside (no bilayer) of the BLV (x-y-z in Figure 8A). This is a consequence of the fact that a cryo-TEM image is a 2D projection of the sample film. The light micrograph in

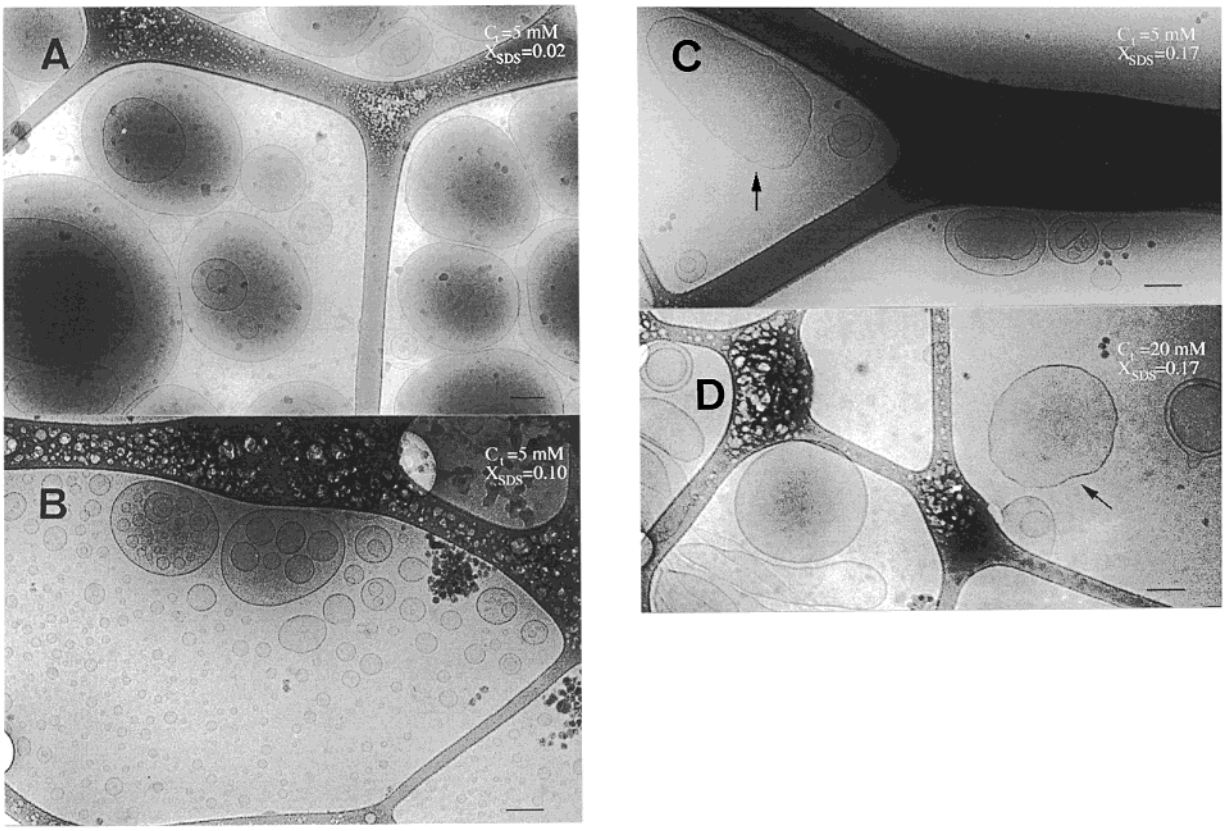

Figure 7. Microstructure of DDAB-rich solutions in the DDAB−SDS−water system obtained by cryo-TEM: (A) $C_t = C_{DDAB} + C_{SDS} = 5$ mM, $X_{SDS} = 0.05$; (B) $C_t = 5$ mM, $X_{SDS} = 0.10$; (C) $C_t = 5$ mM, $X_{SDS} = 0.17$; (D) $C_t = 20$ mM, $X_{SDS} = 0.17$. Arrows indicate undulation of the bilayers. Bar=100 nm.

Figure 8C shows a large number density of giant vesicles of maximum 5 μm in size.

At $X_{SDS} = 0.20$, the sample is a stable monophasic solution, it contains essentially large unilamellar vesicles of 100−400 nm and only very few bilamellar vesicles, as captured by cryo-TEM (Figure 9A). Apparent in the light micrograph in Figure 9B is the fact that the number density of vesicles has decreased substantially, as compared to $X_{SDS} = 0.05$, even though the total surfactant concentration is the same in both samples. No aggregates other than vesicles are visible. The lower density of vesicles at $X_{SDS} = 0.20$ is interpreted as the result of a shift in the size distribution toward substantially lower sizes, i.e., as if a large fraction of the vesicle population is now below the resolution limit of the light microscope ($\approx$0.5 μm). This conclusion is consistent with the larger amount of smaller vesicles captured by cryo-TEM at $X_{SDS} = 0.20$ as compared with $X_{SDS} = 0.05$. As it will be shown below, they are also supported by self-diffusion NMR results.

The microscopy observations for series (i) and (ii) seem to indicate that initial addition of SDS ($X_{SDS} = 0$ to 0.10) causes a large increase in size in the vesicle structures present in solution. Further increase of SDS to values closer to equimolarity ($X_{SDS} = 0.10$ to 0.20) appears to be accompanied by the disintegration of the larger vesicular structures into smaller ones.

b. Water Self-Diffusion. (i) Brief Introduction. To quantify the observations made by the microscopy methods on the effect of SDS on the vesicle size, water self-diffusion measurements were carried out by the PFG−NMR method. This study is analogous to that presented for the SDS-rich solutions of this system[7] and so identical physical considerations therein made regarding water diffusion in polydisperse vesicle solutions apply in this work. In the PFG diffusion experiment, the transport of a molecule is measured over macroscopic distances in the direction of the linear gradient pulse applied. Molecular displacements are measured during the time span Δ (the gradient spacing) which can be varied typically in the range of 1−1000 ms. It is important to differentiate between *free* (Gaussian) diffusion and *restricted* diffusion, in which the molecules experience some sort of boundary for their diffusion on the typical length scales monitored.[30,42,43] For free diffusion, the mean square displacement of the diffusing molecule measured over Δ is given by

$$\langle z^2 \rangle = 2D\Delta \tag{5}$$

where D is the self-diffusion coefficient and the angular brackets indicate a time average. If there are barriers present during the observation time Δ, the net displacement $\langle z^2 \rangle$ is smaller than that of Gaussian diffusion and an apparent D is measured, D_{app}, which is dependent on Δ. In the case of a water solution containing vesicles, the barrier for water diffusion is represented by the vesicle bilayer (a spherical wall). There can be a situation of slow or fast exchange of water between the inside and outside of the vesicle, depending on the relative values of Δ and τ_{res}, the residence time of water inside the vesicles.[7,44] If $\Delta < \tau_{res}$, then a situation of slow exchange is present. The residence time in turn is dependent on the vesicle radius and the permeability coefficient of the membrane for water, P, by

$$\tau_{ves} = R_{ves}/3P \tag{6}$$

In a situation of slow exchange, the water inside the vesicle may experience a situation of restricted diffusion (if $\langle z^2 \rangle^{1/2}$ and R_{ves} are of similar magnitude) and thus a complex Δ-dependent echo-decay appears. Moreover, polydispersity in vesicle size

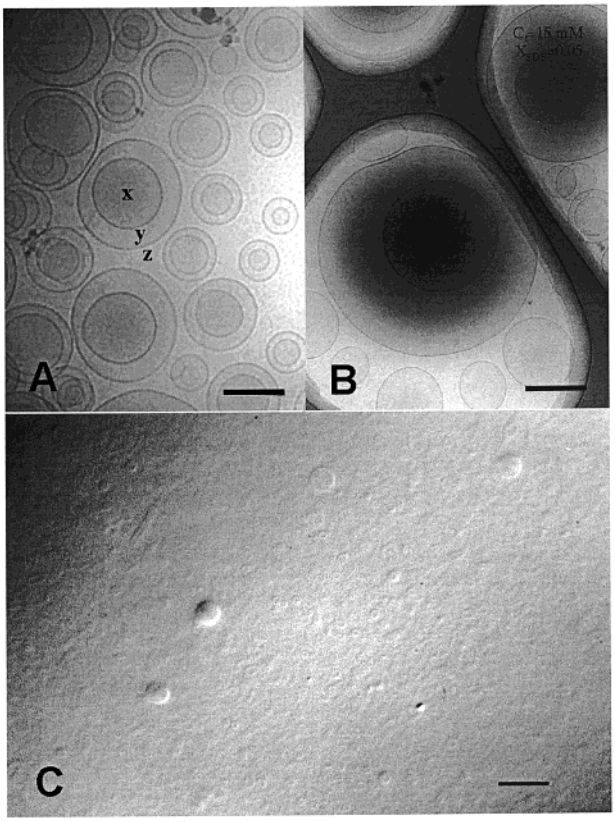

Figure 8. Microstructure for a DDAB-rich solution in the DDAB−SDS−water system at a composition of $C_t = 15$ mM and $X_{SDS} = 0.05$: (A) cryo-TEM micrograph showing large bilamellar vesicles, where x-y-z indicates the differences in mass thickness contrast for 4, 2, or 0 bilayers, respectively; (B) cryo-TEM micrograph showing large unilamellar vesicles (bar = 200 nm); (C) light micrograph showing a high number density of vesicular structures (bar = 10 μm).

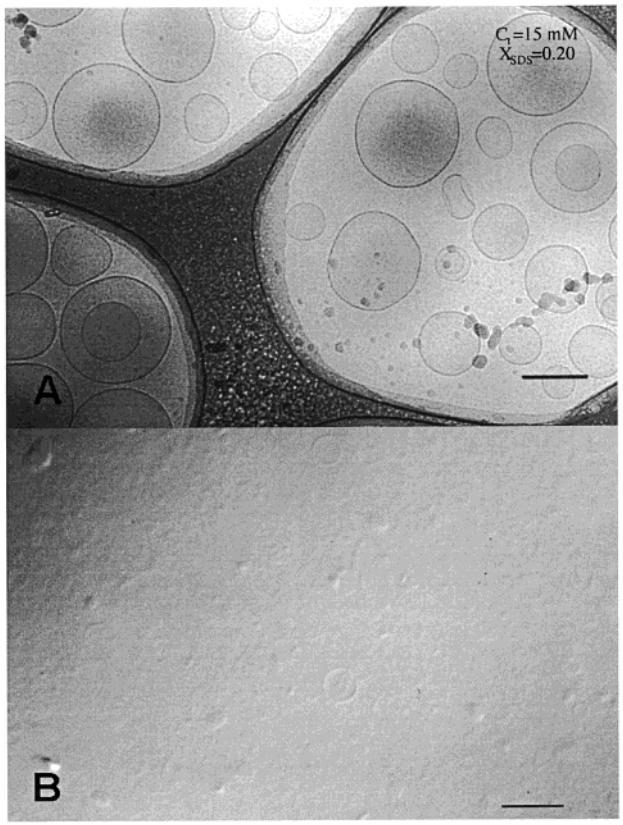

Figure 9. Microstructure for a DDAB-rich solution in the DDAB−SDS−water system at a composition of $C_t = 15$ mM and $X_{SDS} = 0.20$: (A) cryo-TEM micrograph showing essentially LUVs (bar = 200 nm); (B) light micrograph showing a high number density of vesicular structures (bar = 10 μm). Compare this figure with previous one.

may dictate that for a given time, Δ, different segments of the vesicle population are in different regimes of water exchange dynamics,[7] which brings further complexity to the echo profiles.

(ii) Variation of X_{SDS}. In Figure 10 the reduced self-diffusion coefficient (the observed D divided by that of neat water, D_o, at the same temperature) is plotted vs X_{SDS} for four series of samples at different values of constant $C_t = C_{DDAB} + C_{SDS}$. For each series, the measurements were carried out within 1 day after sample preparation and all of the samples were macroscopically homogeneous. After days to weeks, some samples show a thin turbid layer at the top and so they are considered as biphasic samples. The samples which undergo this change are indicated by the dashed diagonal line in Figure 10. It can be seen that for all series of C_t there is a similar trend in the variation of D/D_o with X_{SDS}. There is an initial decrease to some value of X_{SDS}, which is C_t dependent, followed by an increase until the appearance of the catanionic solid. For $C_t = 5$ and 10 mM there is no sharp minimum, while for $C_t =$ 15 and 20 mM it is clear and occurs at low values of X_{SDS} (below 0.05).

For a qualitative confirmation of the trends discussed above, a similar study was done for samples with identical compositions prepared from a sonicated DDAB solution in place of the homogenized dispersion. Ultrasonication of the initially bluish turbid dispersion yields a metastable bluish clear solution. It has been previously reported by Kondo et al. that ultrasonication of 10 mM DDAB dispersions produces unilamellar vesicles of mean radius varying between 40 and 10 nm, depending on the sonication time applied, and that they can remain stable for a few days to weeks without fusion or flocculation (light scattering data).[45,46] From the D/D_o values in Figure 11 obtained for the neat DDAB solutions, one can roughly estimate the mean vesicle size (cf. discussion below in Effect of Dilution within Vesicle Region). Vesicle radius of ca. 9, 30, and 40 nm are obtained for the 10, 15, and 20 mM solutions, respectively, so in reasonable agreement with the cited work[45,46] (note the D/D_o value for 10 mM is very close to unity, yielding a more uncertain value for the radius). The addition of SDS immediately turns the clear solutions into translucent or even turbid solutions, visually indicating a dramatic structural change in the sample. The results for the water diffusion measurements done within 1 day after sample preparation for all series of samples are shown in Figure 11. The trends are rather similar to those seen in Figure 10, but the effects are much more pronounced. In particular, a deep minimum in D/D_o is observed for 15 and 20 mM, corresponding to roughly a 5-fold increase in size with respect to the neat DDAB vesicle (assuming negligible change in average headgroup area upon SDS addition). Another significant observation is that this minimum shifts more markedly to lower X_{SDS} as C_t increases.

The results in Figures 10 and 11 reveal interesting features and appear consistent with the microscopy results. First, we note that a nonexponential, complex echo-decay was obtained for the water diffusion in the samples, with a fast and slow diffusing component being detected (cf. Figure 12a and b, discussed in detail further). The D values used in Figures 10 and 11 correspond then to linear fits to the fast-diffusing component (since the molar fraction of slow-diffusing component is very small, it is discarded). Thus, the D/D_o value is probing the effect of obstruction and entrapment caused by the vesicles to water diffusion, in an situation of fast exchange of water between the interior and exterior of *all* the vesicles in the sample, except

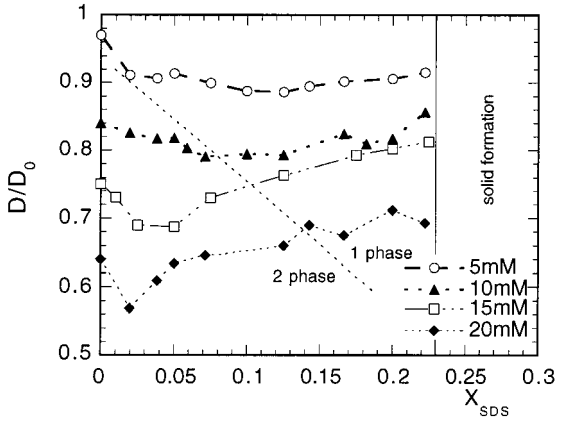

Figure 10. The reduced self-diffusion coefficient of water (D/D_o) vs X_{SDS} for $C_t = C_{DDAB} + C_{SDS} = 5$, 10, 15, and 20 mM. Measurements were done within 1 day after sample preparation; all samples monophasic at time of measurement. The dashed diagonal separates samples which remain as monophasic solutions (1 ph) from those which show a thin turbid layer at the top after a few days (2 ph).

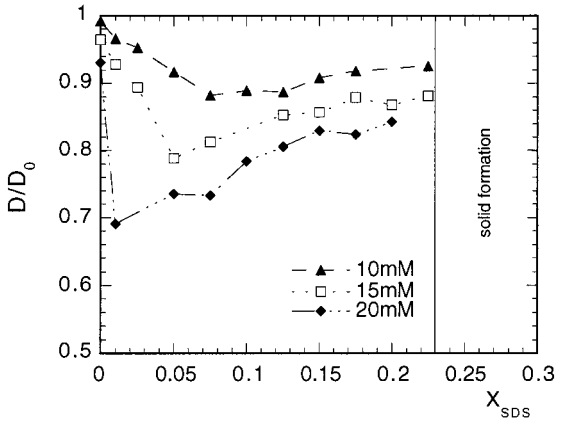

Figure 11. The reduced self-diffusion coefficient of water (D/D_o) vs X_{SDS} for $C_t = 10$, 15, and 20 mM. Samples were prepared from a previously sonicated dispersion of DDAB. Measurements were done within 1 day after sample preparation; all samples monophasic at time of measurement.

for a very small fraction of them.[7] Furthermore, in the case of fast exchange, D/D_o is dependent on the vesicle volume fraction, to first-order approximation, through[47]

$$D/D_o \approx 1 - \frac{3}{2}\Phi_{ves} \qquad (7)$$

The vesicle volume fraction, Φ_{ves}, is in turn a function of vesicle size and vesicle concentration. Thus, in a polydisperse system, changes in vesicle size distribution and particle concentration upon variation of an external parameter can result in a complex variation of D/D_o.

The decrease in D/D_o with the initial X_{SDS} increase is consistent with an increase in the mean size of the vesicles (concomitant with a larger obstructing volume) and entirely in line with the microscopy results shown above. The following increase in D/D_o as X_{SDS} offers more difficulty. It could be interpreted as the result of two opposing effects: (a) decrease in the volume fraction of vesicles associated with a substantial decrease in size and (b) dramatic increase in size of the vesicles in such a way that the rms displacement measured for a large fraction of water molecules is smaller than the vesicle diameter. In this case, the fraction of water would be effectively diffusing freely inside the vesicle and thus contribute to an increase in D/D_o (despite the increase in Φ_{ves}). Since a value of $\Delta = 100$ ms was used, the measured rms displacement for a water molecule is in the order of 10 μm. Situation (b) would thus imply the presence of a significant fraction of vesicles larger than 10 μm. The results from light microscopy do not support this interpretation and, instead, favor the first one. The formation of nonclosed or perforated bilayer structures, which could also explain the increase in D/D_o at higher X_{SDS}, is discarded since we have only evidence for integral vesicle aggregates from the imaging techniques.

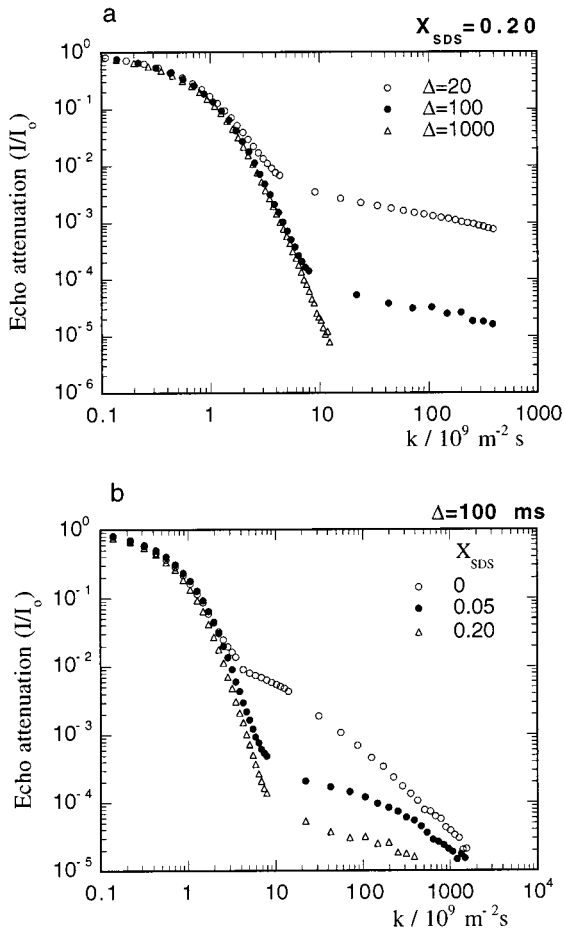

Figure 12. Log−log plots of the echo attenuation of water protons vs k. (a) At $C_t = 15$ mM and $X_{SDS} = 0.20$. Three values of the experimental time scale Δ measured: 20, 100, 1000 ms. For $\Delta = 1000$ ms the slow-diffusing component is no longer present. (b) At constant $\Delta = 100$ ms and increasing X_{SDS}.

(iii) Variation of Experimental Time Scale. A limited investigation of water self-diffusion for the DDAB-rich vesicle solutions/dispersions as a function of the experimental time scale Δ was done. In Figure 12a a log−log plot of the echo-decays vs k as a function of Δ (20, 100, 1000 ms) is presented for the sample at $C_t = 15$ mM and $X_{SDS} = 0.20$, imaged in Figure 9. A nonexponential echo-decay is seen, with presence of a fast-diffusing component, D_{fast}, and a slow-diffusing component, D_{slow}, of rather small molar fraction. This type of profile is representative of the echo-decays obtained for other samples in the system. It is not possible to produce any meaningful fit to the slow-diffusing component. At $\Delta = 1000$ ms, corresponding to an rms displacement of the water molecules of about 30 μm, no slow-diffusing component is detected, i.e., the echo-decay is strictly exponential (Gaussian diffusion). The slow-diffusing water is associated to the water inside the large vesicles, which are in slow exchange.[7] The absence of slow

component at 1000 ms is an indication that *all* of the vesicles are in a regime of fast exchange ($\Delta > \tau_{res}$).

In Figure 12b, diffusion data at $\Delta = 100$ ms is presented for samples with increasing X_{SDS} (Figures 4, 8, and 9). The molar fraction of slow component (f_{slow}) can be obtained by extrapolation of the slow component to $k = 0$ in a log-linear plot. As X_{SDS} increases from 0 to 0.20, f_{slow} gradually decreases, and this can be explained by a gradual decrease of the fraction of the vesicles in solution which are in a slow exchange situation (i.e., the largest vesicles). Thus, on increasing X_{SDS} from 0 to 0.05, the fraction of giant vesicles (in slow exchange) decreases, despite the fact that there is an overall increase in the mean vesicle size. From $X_{SDS} = 0.05$ to 0.20, D_{fast}/D_o increases because of a decrease in mean vesicle size (Figure 10), accompanied also by a decrease in the fraction of large vesicles in the sample (Figure 12b).

With the current data, the observed increase in vesicle size followed by a decrease beyond a critical value of X_{SDS} can only be rationalized at a qualitative level. The trend reveals in an interesting way the complexity of the interactions between the two surfactants in the aggregate and, also, of the interaggregate interactions, which depend critically on such factors such as salt concentration (NaBr in this case) and volume fraction of particles. As mentioned before, when the anionic surfactant SDS is added to the cationic DDAB bilayer aggregates, two opposing effects appear. Electrostatic attractions between the surfactant headgroups favor the formation of aggregates with lower positive mean curvature, i.e., favor an increase in aggregate size. However, packing constraints due to the introduction of a single-chained surfactant in the bilayer favor higher positive mean curvature, i.e., a decrease in aggregate size. The predomination of one of the effects over the other should be dependent on the surfactant mixing ratio (and thus, concentration of salt) and total surfactant concentration.

At low values of X_{SDS} the electrostatic effects dominate and an increase in mean vesicle size can be reasonably accounted for. At high enough mole fraction of SDS in the aggregate, where electrostatics is less dominant, packing effects appear to dominate and favor the breakage of large vesicles into smaller ones. As the total surfactant concentration is increased, a higher amount of salt is present in the system and also a higher vesicle volume fraction exists, implying less available volume for the initial growth. These effects could lie behind the other observed trend—the lowering of the X_{SDS} value for maximum mean vesicle size as C_t rises.

3. Effect of Dilution within Vesicle Region. The cryo-TEM observation indicates that no significant structural changes are induced by diluting a sample at fixed X_{SDS} within the vesicle region. This fact is illustrated for a series of samples investigated at $X_{SDS} = 0.17$, diluted between 0.77 and 0.2 wt % DDAB, i.e., by a 4-fold factor (Figs 7C and 7D). Indeed, diluting sample D to C does not bring about a significant change in type of aggregates present or mean vesicle size. Large unilamellar vesicles are the dominating aggregates for both samples. Further confirmation is obtained from the diffusion data below.

In Figure 13 the values obtained for D/D_o for samples also at constant $X_{DDAB} = 0.17$, along a dilution path ($C_t = 2.5$ to 20 mM) in the isotropic solution, are shown. Assuming (i) the existence of vesicle monodispersity, (ii) that the vesicles behave as hard spheres and are not too small, and (iii) a situation of fast exchange is present, the vesicle volume fraction Φ_{ves} can be obtained from D/D_o by

$$\Phi_{ves} = 2(1 - D/D_o)/(2 + D/D_o) \qquad (8)$$

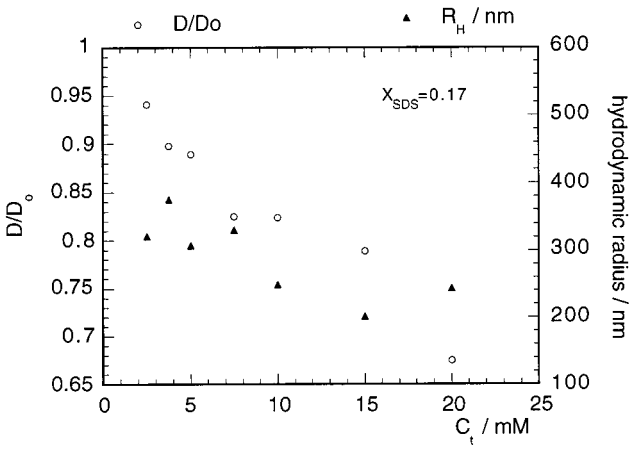

Figure 13. Estimation of vesicle sizes from the reduced self-diffusion coefficient of water (D/D_o) along a dilution path at $X_{SDS} = 0.17$ within the DDAB-rich vesicle region.

An estimation of the vesicle radius can then be obtained by use of

$$R_{ves} = \frac{6\Phi_{ves}}{N_A C_t a_s} \qquad (9)$$

where N_A is Avogadro's number, C_t is the total surfactant molar concentration, and a_s is the average surfactant headgroup area. A value of average headgroup area per surfactant $a_s = 0.50$ nm^2 was used in eq 9. This value was chosen on the basis of the sample composition $C_{DDAB}/C_{SDS} = 5{:}1$ and assuming that the minimal cross-section area per chain, 0.25 nm^2, is a limiting value for headgroup area minimization. From the diffusion data in Figure 13, the vesicle sizes obtained are in the order of 250−350 nm. Moreover, along a dilution path there is not a significant change in vesicle size, which indicates an approximately linear decrease of vesicle volume fraction with decreasing surfactant concentration. Overall, these results are rather consistent with the observations made with cryo-TEM.

IV. Summary and Final Remarks

In the binary double-chained surfactant−water system, a solution region of vesicles can be found only at very low surfactant concentration. It has been shown that the addition of the anionic surfactant SDS to the system extends the single phase region of vesicles to higher total surfactant concentration. The DDAB-rich catanionic vesicles are characterized in general by large sizes and high polydispersity. Large and giant unilamellar vesicles in the range of 200−1000 nm are detected by electron microscopy. Light microscopy also indicates the presence of large vesicular structures in the range of 1−10 μm. The average vesicle size and degree of polydispersity are thus much larger than for the vesicles forming in the SDS-rich side of the mixture, a direct consequence of the difference in the packing parameter of the two surfactants. Overall, the DDAB−SDS−water mixture provides a system in which the net charge, mean size of the vesicles, and vesicle volume fraction are to some extent controllable, through surfactant concentration and mixing ratio.

The observed changes in phase behavior and phase microstructure in the DDAB-rich side can be summed up by looking at the system from the viewpoint of adding excess cationic surfactant to the equimolar mixture. It has been seen that equimolarity leads to associative phase separation, with formation of the catanionic solid DDA^+DS^- in the presence of a salt solution. The introduction of net charge in the catanionic system,

by DDAB addition, has a large effect on phase behavior, destabilizing the precipitate and inducing the formation of vesicular solutions. This type of phase behavior is similar to that observed for the anionic-rich side, and is in fact a typical trend for catanionic mixtures. Microscopy and water self-diffusion data suggest that the size and degree of polydispersity of the vesicles in the system vary in a nonmonotonic way with the excess amount of double-chained amphiphile. At low amount of excess DDAB, where higher salt concentration is present and thus the role of electrostatics reduced, there appears to be a domination of packing effects by the single-chained SDS. As a consequence, vesicular aggregates of lower average size are present. At higher excess of DDAB, electrostatics dominate over the packing effects and, thus, larger structures are detected. The self-diffusion data also imply the existence of a critical mixing ratio for which the mean size attains a maximum. Possible ways of fully elucidating the trends observed in this system, in particular the interplay between electrostatic and curvature constraints, would be (i) to monitor the structure and phase behavior of the catanionic system in the presence of added salt or (ii) to carry on a comparative microscopy and self-diffusion study for mixtures of DDAB with other surfactants (anionic, cationic, nonionic). Work on this issues is currently in progress.

Acknowledgment. Håkan Wennerström and Andrew Fogden are acknowledged for valuable discussions. E.F.M. is grateful to Praxis XXI (F.C.T., Portugal) for a research grant (ref. BD/9295/96). O.R. acknowledges a grant from the Swedish Institute for his stay in Lund. The Swedish Research Council for Engineering Sciences (TFR) and Praxis XXI (project 2/2.1/QUI/411/94) are also gratefully acknowledged for financial support.

References and Notes

(1) Kaler, E. W.; Murthy, A. K.; Rodriguez, B. E.; Zasdzinski, J. A. N. *Science* **1989**, *245*, 1371.
(2) Kaler, E. W.; Herrington, K. L.; Murthy, A. K.; Zasadzinski, J. A. *J. Phys. Chem.* **1992**, *96*, 6698−6707.
(3) Ambühl, M.; Bangerter, E.; Luisi, P. L.; Skrabal, P.; Watzke, H. J. *Prog. Colloid Polym. Sci.* **1993**, *93*, 183.
(4) Watzke, H. J. *Prog. Colloid Polym. Sci.* **1993**, *93*, 15.
(5) Kondo, Y.; Uchiyama, H.; Yoshino, N.; Nihyiama, K.; Abe, M. *Langmuir* **1995**, *11*, 2380.
(6) Khan, A.; Marques, E. Catanionic Surfactants. In *Specialists Surfactants*; Robb, I. D., Ed.; Blackie Academic and Professional, an imprint of Chapman & Hall: London, 1997; pp 37.
(7) Marques, E. F.; Regev, O.; Khan, A.; Miguel, M. G.; Lindman, B. *J. Phys. Chem. B* **1998**, *102*, 6746.
(8) Safran, S. A.; Pincus, P.; Andelman, A.; Mackintosh, F. C. *Phys. Rev.* **1991**, *43*, 1071.
(9) Bergström, M. *Langmuir* **1996**, *12*, 2454.
(10) Yuet, P. K.; Blankschtein, D. *Langmuir* **1996**, *12*, 3802.
(11) Israelachvili, J. N. *Intermolecular and Surface Forces*, 2nd ed.; Academic Press: San Diego, 1992.
(12) Evans, D. F.; Wennerström, H. *The Colloidal Domain: Where Physics, Chemistry, Biology and Technology Meet*; VCH: New York, 1994.
(13) Fontell, K.; Ceglie, A.; Lindman, B.; Ninham, B. *Acta Chem. Scand.* **1986**, *A40*, 247.
(14) Warr, G. G.; Sen, R.; Evans, D. F.; Trend, J. E. *J. Phys. Chem.* **1988**, *92*, 774.
(15) Dubois, M.; Zemb, T. *Langmuir* **1991**, *7*, 1352.
(16) Zemb, T.; Gazeau, D.; Dubois, M.; Gulik-Krzywicki, T. *Europhys. Lett.* **1993**, *21*, 759.
(17) Brady, J. E.; Evans, D. F.; Warr, G. G.; Grieser, F.; Ninham, B. W. *J. Phys. Chem.* **1986**, *90*, 1853.
(18) Miller, D. D.; Bellare, J. R.; Evans, D. F.; Talmon, Y.; Ninham, B. W. *J. Phys. Chem.* **1987**, *91*, 674.
(19) Dubois, M.; Gulik-Krzywicki, T.; Cabane, B. *Langmuir* **1993**, *9*, 673.
(20) Regev, O.; Khan, A. *Prog. Colloid Polym. Sci.* **1994**, *97*, 298.
(21) Svitova, T. F.; Smirnova, Y. P.; Pisarev, S. A.; Berezina, N. A. *Colloids Surf. A* **1995**, *101*, 107.
(22) Edwards, K.; Gustafsson, J.; Almgren, M.; Karlsson, G. *J. Colloid Interface Sci.* **1993**, *161*, 299.
(23) Inoue, T. Interaction of surfactants with phospholipid vesicles. In *Vesicles*; Rosoff, M., Ed.; Marcell Dekker: New York, 1996; p 151.
(24) Silvander, M.; Karlsson, G.; Edwards, K. *J. Colloid Interface Sci.* **1996**, *179*, 104.
(25) Van de Pas, J. C. *Tenside Surf. Det.* **1991**, *28*, 158.
(26) Kachar, B.; Evans, D. F.; Ninham, B. W. *J. Colloid Interface Sci.* **1984**, *100*, 287.
(27) Bellare, J. R.; Davis, H. T.; Scriven, L. E.; Talmon, Y. *J. Electron Microsc. Technol.* **1988**, *10*, 87.
(28) Vinson, P. K. "Cryo-TEM, carbon-coated holey polymer film"; The 45th Annual Meeting of the Electron Microscopy Society of America, 1987, San Francisco.
(29) Stilbs, P. *Prog. Nucl. Magn. Reson. Spectrosc.* **1987**, *19*, 1.
(30) Price, W. S. *Concepts Magn. Res.* **1997**, *9*, 299.
(31) Laughlin, R. G. Aqueous Phase Science of Cationic Surfactant Salts. In *Cationic Surfactants-Physical Chemistry*; Rubingh, D. N., Holland, P. M., Eds.; Marcell Dekker: New York, 1991.
(32) Zemb, T.; Belloni, L.; Dubois, M.; Marcelja, S. *Progr. Colloid. Polym. Sci.* **1992**, *89*, 33.
(33) Caria, A.; Regev, O.; Khan, A. *J. Colloid Interface Sci.* **1998**, *200*, 19.
(34) Israelachvili, J. N.; Mitchell, D. J.; Ninham, B. W. *J. Chem. Soc., Faraday Trans. 2* **1976**, *72*, 1525.
(35) Evans, D. F.; Mitchell, D. J.; Ninham, B. J. *J. Phys. Chem.* **1986**, *90*, 2817.
(36) Feitosa, E., personnal communication.
(37) Regev, O.; Kang, C.; Khan, A. *J. Phys. Chem.* **1994**, *98*, 6619.
(38) Evans, D. F.; Ninham, B. W. *J. Phys. Chem.* **1986**, *90*, 226.
(39) Caboi, F.; Monduzzi, M. *Langmuir* **1996**, *12*, 3548.
(40) Marques, E.; Khan, A.; Miguel, M. G.; Lindman, B. *J. Phys. Chem.* **1993**, *97*, 4729.
(41) Dubois, M.; Zemb, T.; Belloni, L.; Delville, A.; Levitz, P.; Setton, R. *J. Chem. Phys.* **1992**, *96*, 2278.
(42) Söderman, O.; Stilbs, P. *Prog. Nucl. Magn. Reson. Spectrosc.* **1994**, *26*, 445.
(43) Söderman, O.; Olsson, U. *Curr. Opinion Colloid Interface Sci.* **1997**, *2*, 131.
(44) Olsson, U.; Nakamura, K.; Kunieda, H.; Strey, R. *Langmuir* **1996**, *12*, 3045.
(45) Kondo, Y.; Abe, M.; Ogino, K.; Uchiyama, H.; Tucker, E. E.; Scamehorn, J. F.; Christian, S. D. *Colloids Surf. B* **1993**, *1*, 51.
(46) Kondo, Y.; Abe, M.; Ogino, K.; Uchiyama, H.; Scamehorn, J. F.; Tucker, E. E.; Christian, S. D. *Langmuir* **1993**, *9*, 899.
(47) Söderman, O.; Herrington, K. L.; Kaler, E. W.; Miller, D. D. *Langmuir* **1997**, *13*, 5531.